ARTICLE

The Role Radius of Curvature Plays in Thiolated Oligonucleotide Loading on Gold Nanoparticles

Haley D. Hill, Jill E. Millstone, Matthew J. Banholzer, and Chad A. Mirkin*

Department of Chemistry and International Institute of Nanotechnology, Northwestern University, 2145 Sheridan Road, Evanston, Illinois 60208-3113

ABSTRACT We show that by correlating the radius of curvature of spherical gold nanoparticles of varying sizes with their respective thiol-terminated oligonucleotide loading densities, a mathematical relationship can be derived for predicting the loading of oligonucleotides on anisotropic gold nanomaterials. This mathematical relationship was tested with gold nanorods (radius 17.5 nm, length 475 nm) where the measured number of oligonucleotides per rod (3330 ± 110) was within experimental error of the predicted loading of 3244 oligonucleotides from the derivation. Additionally, we show that once gold nanoparticles reach a diameter of approximately 60 nm the local surface experienced by the oligonucleotide is highly similar to that of a planar surface.

KEYWORDS: gold nanoparticle · curvature · DNA-functionalized · gold nanorod · loading

Polyvalent oligonucleotide gold nanoparticle conjugates (oligo-AuNPs) are being extensively used in the development of therapeutic, diagnostic, and spectroscopic applications.[1−5] The reasons these structures have found such widespread use are that they can be easily synthesized and chemically modified, exhibit intense surface plasmon resonances ($\varepsilon > 3 \times 10^8$ L/(mol · cm)),[2] have catalytic properties distinct from their bulk counterparts, and are generally stable in the context of diagnostic probe and therapeutic applications.[6−8] The surface coverage of oligonucleotides on spherical or highly faceted gold nanoparticles, which is oftentimes much greater than other particle compositions (*e.g.*, silica, polystyrene),[9] leads to unusually high electrostatic and steric stabilization of the particles and their ability to engage in highly cooperative hybridization interactions with complementary nucleic acids.[9,10] The high loading of oligonucleotides on gold nanoparticles derives from (1) the substitutionally labile coordination sphere of citrate ions adsorbed onto the surfaces of the particle precursors used to prepare the oligo-AuNPs, (2) the thiol-gold chemistry used to surface immobilize the oligonucleotides, (3) the salt-induced aging procedures used to decrease electrostatic interactions between neighboring oligonucleotides, and (4) the radius of curvature of the particles. The first three factors are constant regardless of particle size, whereas radius of curvature is highly dependent upon the dimensions of the particle.

These observations make one question, when do the surface modification properties and capacity for adsorbate loading of a particle begin to resemble those of a planar surface? This question has been considered for uncharged hydrophobic alkanethiols on Au clusters by Landman *et al.*, but not for chemically more sophisticated structures like oligonucleotides on larger gold nanoparticles (>2 nm).[11,12] Charged multifunctional adsorbates like oligonucleotides likely will follow a similar trend but have a greater number of variables, which significantly affect their packing behavior. Herein, we present a study of oligo-AuNPs made from Au cores ranging in diameter from 10 to 200 nm and aimed at determining how the radius of curvature of a particle influences oligonucleotide surface coverage. We compare these results to values obtained from planar gold surfaces and identify the nanoparticle size that begins to mimic the properties of a planar substrate. We then evaluate how these numbers and geometric models can be used to predict the oligonucleotide surface coverage for anisotropic rod-shaped particles.

RESULTS

Surface Oligonucleotide Loading as a Function of Salt Concentration. Previous work by our group and others has shown that the sur-

See the accompanying Perspective by Cederquist and Keating on p 256.

*Address correspondence to chadnano@northwestern.edu.

Received for review October 31, 2008 and accepted December 15, 2008.

Published online January 15, 2009.
10.1021/nn800726e CCC: $40.75

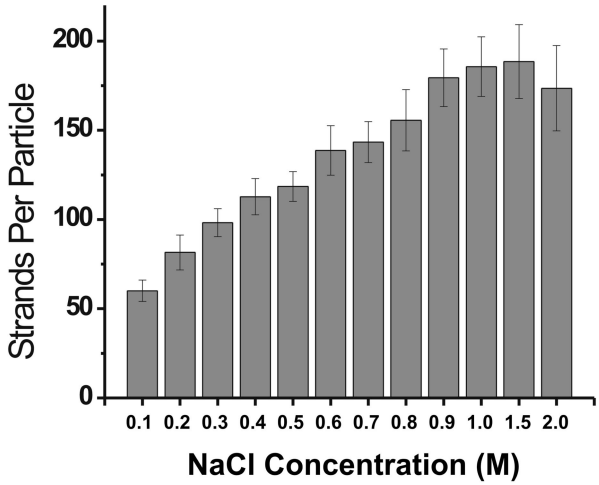

Figure 1. Oligonucleotide loading as a function of salt concentration for 20 nm AuNPs. The error bars indicate the standard deviation of five independent measurements.

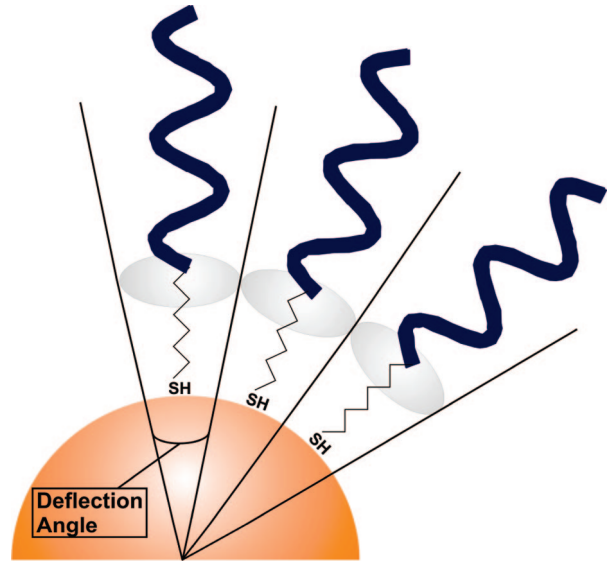

Scheme 1. Drawing illustrating how the radius of curvaure of the AuNP affects the interaction between neighboring oligonucleotide strands. This interaction is represented by the deflection angle between the oligonucleotides.

face loading of oligonucleotides increases with increasing salt concentration.[8,10] To evaluate the optimum salt concentration for loading oligonucleotides on Au nanoparticle surfaces, we measured surface loading for 20 nm diameter particles as a function of successively increasing salt concentration (Figure 1). One observes a steady rise in loading up to about 1 M NaCl concentration, after which loading levels off. Therefore, we chose this salt concentration as a constant for all subsequent measurements.

Surface Density of Oligonucleotides as a Function of Nanoparticle Radius. The surface density of oligonucleotides for each particle size was calculated by dividing the number of oligonucleotides per particle by the calculated surface area (nm^2) (Table 1, column 2). Several assumptions regarding surface area were made. First, the nanoparticles were modeled as perfect spheres. Second, the numbers of particles larger and smaller than the average particle size were assumed to be equal. Third, the oligonucleotides were assumed to be evenly distributed on the nanoparticle surface. As predicted, the surface curvature significantly affects the loading of oligonucleotides with smaller particle sizes exhibiting higher coverages than larger diameter structures. From these data, one can see that, when the particles reach a diameter of approximately 60 nm (and certainly above 100 nm), the surface coverage remains nearly constant for all particle sizes above this value and is comparable to values determined for a planar gold substrate (Figure 2).

The effective DNA footprint (K) is one way to think about the spatial arrangement of oligonucleotides on the nanoparticle surface. Footprint is defined as the average area each oligonucleotide occupies on the nanoparticle surface (Table 1, column 3; eq 1).

$$\text{footprint}: K\left(\frac{\text{nm}^2}{n}\right) = \left[\frac{4\pi r^2}{N_r}\right] \qquad (1)$$

K represents the average area each oligonucleotide occupies on the nanoparticle surface in nm^2 (footprint), and *N* represents the average number of oligonucle-

TABLE 1. Average Values Including Standard Deviations for Particle Sizes, Absolute Number of Oligonucleotides Per Particle, Surface Coverage, Effective Footprint, and Calculated Deflection Angle

diameter (nm)	oligos/particle	coverage (oligos/cm^2)	footprint (nm^2)	deflection (deg)
10	68 ± 10	$2.0 \times 10^{13} \pm 2 \times 10^{12}$	4.9 ± 1	29 ± 3
15	110 ± 10	$1.7 \times 10^{13} \pm 2 \times 10^{12}$	6.0 ± 1	21 ± 2
20	180 ± 20	$1.4 \times 10^{13} \pm 1 \times 10^{12}$	7.0 ± 1	17 ± 2
30	260 ± 10	$9.3 \times 10^{12} \pm 8 \times 10^{11}$	11 ± 1	14 ± 1
40	430 ± 10	$8.5 \times 10^{12} \pm 4 \times 10^{11}$	12 ± 2	11 ± 2
50	640 ± 80	$8.1 \times 10^{12} \pm 3 \times 10^{11}$	12 ± 1	9.0 ± 1
60	890 ± 20	$7.8 \times 10^{12} \pm 1 \times 10^{12}$	13 ± 2	7.7 ± 1
80	1400 ± 100	$7.1 \times 10^{12} \pm 9 \times 10^{11}$	14 ± 2	6.1 ± 1
100	2200 ± 200	$7.1 \times 10^{12} \pm 4 \times 10^{11}$	14 ± 1	4.9 ± 1
150	5100 ± 100	$7.1 \times 10^{12} \pm 2 \times 10^{11}$	14 ± 2	3.2 ± 1
200	8500 ± 200	$6.8 \times 10^{12} \pm 1 \times 10^{12}$	15 ± 2	2.5 ± 1
planar gold	N/A	$5.8 \times 10^{12} \pm 7 \times 10^{11}$	18 ± 2	0

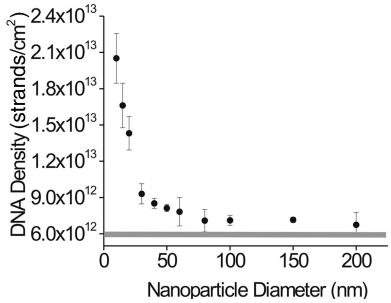

Figure 2. Oligonucleotide density determined as a function of AuNP diameter. The gray line represents oligonucleotide loading on a planar gold surface.

otides per particle for a given radius, *r* (Scheme 2A).

Calculating the Average Deflection Angle between Oligonucleotides. The average deflection angle between oligonucleotides attached to the AuNP is directly related to the radius of curvature of the nanoparticle and illustrates the spatial arrangement of the strands as well as how this arrangement is dependent upon the AuNP radius (Scheme 1). To calculate the deflection angle between two oligonucleotides on the nanoparticle surface, the above assumptions were used, along with two additional ones. For these calculations, we assume that the oligonucleotides adopt a rod-like orientation. To test the validity of this assumption, dynamic light scattering measurements were used to determine the approximate length of the oligonucleotides attached to the AuNPs (Figure 3). On average, the oligonucleotides were estimated to be 9 nm in length, similar to the expected value if modeled as rod-like, extended structures (rod-like ssDNA, approximately 10 bases/3 nm, is expected to be shorter than fully outstretched 13.4 nm long single-stranded DNA due to coiling).[13,14] Additionally, we modeled the oligonucleotide footprint as a circular area (Scheme 2B) which was used to calculate the deflection angle between oligonucleotides using eqs 2 and 3:

$$R = \sqrt[2]{\frac{K}{\pi}} \tag{2}$$

$$\text{Deflection (deg)} = \left[\frac{2R}{r}\right] \times \frac{180}{\pi} \tag{3}$$

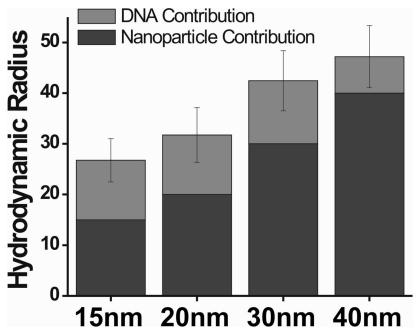

Figure 3. Diameter determined by dynamic light scattering measurements. The values presented above are the average of three separate measurements.

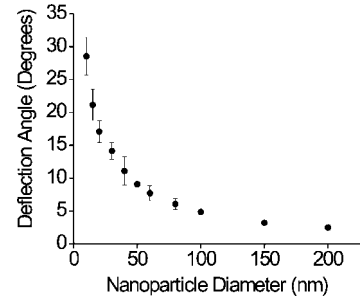

Figure 4. Oligonucleotide deflection angle as a function of AuNP diameter.

where *R* represents the radius of the footprint approximation on the nanoparticle surface, *K* is the footprint of the oligonucleotide on the AuNP surface, and *r* is the average radius of the nanoparticle. Deflection angles were determined for all particle sizes studied and planar gold (Table 1, column 5, and Figure 5).

Deriving an Equation for Predicting the Loading of Oligonucleotides on Gold Nanorods. Quantitatively predicting surface coverage for a rod is more difficult than a sphere. A rod is a cylindrical body with two flat ends.[15] One must take this geometry into account with weighted contributions from the curved and planar portions of the structure. The surface area of a rod can be calculated using eq 4:

$$\text{SA(rod)} = 2\pi r^2 + 2\pi rl \tag{4}$$

where *r* is the radius of the rod and *l* is the length of the rod. To approximate the number of oligonucleotides on the rod, the two end segments (represented by $2\pi r^2$) were assumed to be flat planar surfaces where oligonucleotides have an average footprint of 17.5 nm^2. While they are not perfectly flat (rms roughness $\sim$ 15 nm), AFM studies show that these are best modeled as flat rather than curved surfaces.[15] Second, we did not include contributions from adsorption of oligonucleotides on the edges of the cylinder ends. Third, we approximated the footprints of the oligonucleotides on the outer wall of the cylinder (not the ends) as an ellipse. To do this, we used the radius of the nanorod to assign a spacing parameter for oligonucleotides attached to the curved surface of the rod in bands (Scheme 3). The data presented in Table 1 were used to relate the radius of a nanoparticle to the average footprint diameter for an oligonucleotide around the circumference of the rod. This derivation yielded the relationship shown in eq 5.

$$\text{Length of Ellipse (nm)} = 2 * \sqrt[2]{\frac{3.3618 \ln r + 0.1616}{\pi}} \tag{5}$$

To estimate the spacing down the long axis of the rod, we assumed that the oligonucleotides experienced a situation similar to a flat surface, where the

spacing was 4.72 nm per oligonucleotide. The total surface area of the entire rod was then divided into oligonucleotide footprint domains to approximate the number of oligonucleotides that can pack on a nanorod of a given length and radius (eq 6):

$$\frac{\text{Oligonucleotides}}{\text{rod}} = \frac{2\pi r^2}{17.55} + \frac{2\pi r}{2 * \sqrt[2]{\frac{3.3618 \ln r + 0.1616}{\pi}}} * \frac{l}{4.72} \quad (6)$$

where r is the radius of the rod and l represents the length of the rod (Scheme 3).

While oligo-AuNPs with average gold core diameters varying from 2 to 250 nm have been prepared and studied previously,[10,16] the majority of studies have focused on the 13−15 nm range, typically functionalized with oligonucleotides containing 25−35 bases.[17−25] Therefore, for this study, we chose 15 nm diameter particles, modified with a 25 base sequence as a representative example (5′-HS-AAA AAA AAA AAA TAT TGA TAA GGA T-FITC-3′). If one considers that a 15 nm gold particle has a radius of 7.5 nm and compares that to the persistence length of a 25 bp oligonucleotide at approximately 8.5 nm (where 10 base pairs are approximately equivalent to 3 nm),[13] an interesting observation is made: the dimensions of the two are essentially the same. This prompted us to consider the spatial relationship of the gold nanoparticle and the oligonucleotides attached to its surface from a geometric perspective. If one approximates a 15 nm AuNP as a sphere and envisions oligonucleotides attached to the particle surface at one end through a chemical linker (Au−S), one can make a few key observations (Scheme 1). First, the distance between the oligonucleotide strands is closest at the particle surface and grows larger as the chain extends from the surface (Scheme 1). Second, as particle radius increases, one must move further from the particle surface to maintain comparable inter-oligonucleotide distances. Third, as particle size increases, eventually the oligonucleotides attached to it begin to more closely resemble the spacing of oligonucleotides attached to a flat surface. Thus far, the magnitude of these effects has never been studied, and the particle size that begins to mimic the properties of a flat surface has not been identified.

DISCUSSION

A goal of this work is to determine how changes in the surface curvature of gold nanoparticles affect the organization of thiol-terminated oligonucleotides attached at their surfaces. Initially, we hypothesized that thiol-terminated oligonucleotides attached to relatively small AuNPs (less than 20 nm diameter) would have significantly more distance between the neighboring strands moving radially out from the surface than their

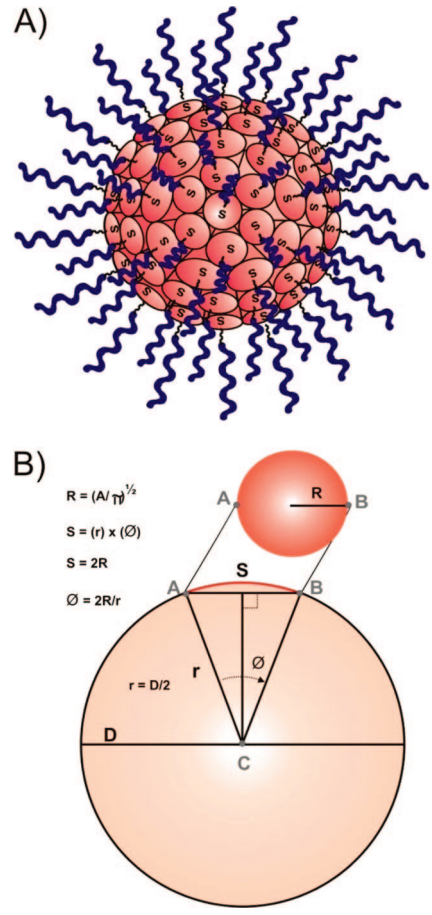

Scheme 2. Model of the oligonucleotide-modified AuNP surface. (A) Model used to calculate the oligonucleotide footprint. (B) Illustration of how the footprint from (A) is used to approximate the deflection angle.

larger particle counterparts, resulting from the smaller particles highly curved surfaces. This should decrease steric interactions between oligonucleotides attached to small AuNPs, thus allowing for more oligonucleotides to attach to the highly curved surface than to the larger flatter surfaces, when equal areas are compared (Figure 2). Indeed, our data confirm that the loading of oligonucleotides on AuNPs, smaller than 20 nm show a dramatic increase in oligonucleotide surface coverage when compared to their larger counterparts. However, when the diameter exceeds 60 nm, the oligonucleotide surface coverage approaches the values obtained for a flat gold surface (Figure 2 and Table 1).

Another way to look at this relationship is to directly compare the estimated deflection angles be-

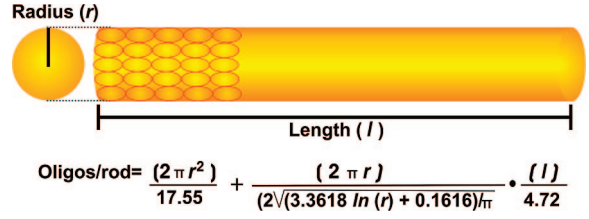

Scheme 3. Model of oligonucleotide packing on a gold nanorod surface.

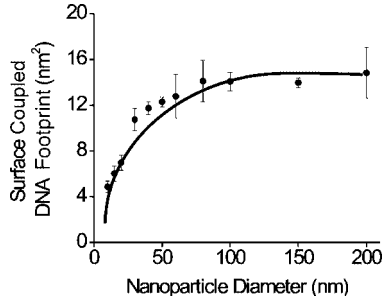

Figure 5. Oligonucleotide footprint as a function of AuNP diameter.

tween the strands as calculated above (Scheme 1). This comparison shows that the deflection between the strands is greatest on the smallest particles and exponentially decays to almost no deflection for the largest particles (Figure 4). Oligonucleotides on planar gold surfaces exhibit more regular packing and a salt concentration-dependent tilt angle, but do not exhibit a relative deflection angle.[26]

One of the goals this work was to derive a mathematical relationship that can be used to predict the loading of similar oligonucleotides on anisotropic gold nanostructures. Therefore, we needed to determine the effective footprint of an oligonucleotide (surface area occupied) as a function of particle curvature. Our results show that as nanoparticle diameter decreases and curvature increases effective footprint decreases (Figure 5). This relationship is the foundation of our rod loading derivation (Scheme 3). The loading experiments show that one can quantitatively predict saturated oligonucleotide surface coverages for gold nanorods (Figure 6). Indeed, the experimentally determined value of 3330 ± 114 corresponds remarkably well with the predicted value of 3244 oligonucleotides per rod.

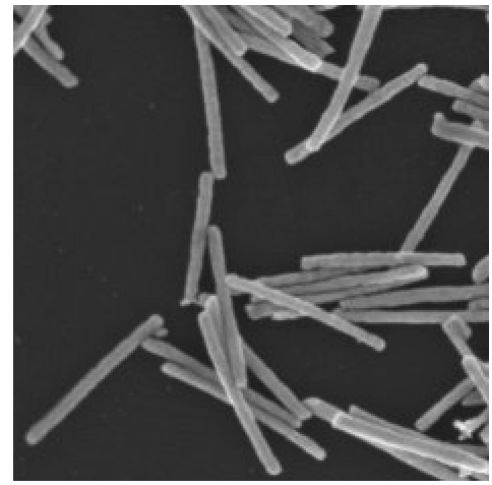

Figure 6. SEM of representative gold nanorods; average diameter = 35 ± 5 nm and average length = 475 ± 33 nm. The image displayed above shows a 1.5 × 1.5 μm area.

This work provides a way of understanding and predicting oligonucleotide surface coverage on nanoparticles as a function of curvature, shape, and available surface area. Indeed, the data provided are the first quantitative measures of the relationship between particle curvature and oligonucleotide loading. The results show that as particle diameter increases to 60 nm it begins to mimic the properties of a planar surface, and above 100 nm, it behaves virtually identically to a planar surface in terms of oligonucleotide loading. Additionally, we show that the loading of oligonucleotides on gold nanorods can also be accurately predicted using this curvature relationship. Importantly, the geometric models worked out in this paper, in principle, could be adapted for many particle shapes simply by using the different geometric equations for surface area.

EXPERIMENTAL METHODS

Materials. Gold nanoparticles (10, 15, 20, 30, 40, 50, 60, 80, 100, 150, and 200 nm diameter) were purchased from Ted Pella, Inc. (Redding CA) and used as received. All oligonucleotides were synthesized on an ABI Expedite nucleic acid synthesizer using standard phosphoramidite chemistry[27] with reagents from Glen Research Corporation (Sterling, VA). All oligonucleotides were purified by reverse phase high-pressure liquid chromatography on an Agilent 1100 HPLC (Santa Clara, CA). Sodium chloride (NaCl), sodium phosphate (Na_2HPO_4 and NaH_2PO_4, PB), sodium dodecyl sulfate (SDS) and dithiothreitol (DTT) were molecular biology grade, purchased from Sigma Aldrich (Milwaukee, WI) and used as received. NAP-5 columns were obtained from GE Healthcare (Piscataway, NJ) and used for all desalting procedures. All experiments were done using Nanopure water (Barnstead Int., Dubuque, IA). Anodic aluminum oxide templates were obtained from Synkera Technologies Inc. Metal plating solutions were obtained from Technic, Inc. and used as received.

Gold Nanorod Synthesis and Characterization. Nanorods were fabricated using an electrochemical, template-directed method.[28,29] Briefly, a 125 nm Ag backing was thermally evaporated onto one side of an anodic aluminum oxide (AAO) membrane (35 nm pore diameter, 13 mm membrane diameter, Synkera Technologies Inc.), which served as a working electrode during the electrodeposition growth process. The template was placed in an electrochemical cell with a platinum counter electrode and a Ag/AgCl reference electrode. A 1025 silver RTU solution (Technic, Inc.) was diluted by a factor of 3 with water and used to plate a silver section into the AAO template (−800 mV *vs* Ag/AgCl). This silver section served as a "buffer layer" to create more uniform electrical contacts, which results in more uniform gold rods (~3 C, 1−3 μm in length depending on contact between evaporated silver backing and AAO membrane). After deposition of this buffer segment, the Ag plating solution was removed and the electrochemical cell was rinsed with water for 3 min. Next, a solution of Orotemp 24 gold RTU plating solution (Technic, Inc., diluted by a factor of 3 with water) was used to grow the gold nanorods at −900 mV *vs* Ag/AgCl (485 mC of charge was passed to generate approximately 500 nm long gold rods). After the electrodeposition was completed, the membrane was placed in concentrated HNO_3 (40 min) to dissolve the silver backing and buffer layer. The mixture was then rinsed and sonicated in NaOH (3 M) to dissolve the AAO template (30 min). The resulting nanorods were rinsed first with water (3×), then ethanol (3×), and finally with water (3×). The resulting rods were then characterized by scanning electron microscopy (LEO 1525 FE-SEM, 3 kV)

in order to determine their dimensions (*d*) = 35 ± 5.3 nm; length (*l*) = 475 ± 33 nm).

Oligonucleotide Functionalized Gold Nanoparticle Preparation. Oligonucleotide functionalized gold nanoparticles were prepared following literature procedures.[10] All procedures were conducted in the dark to prevent photobleaching of the fluorescein dye (FITC). Briefly, lyophilized oligonucleotides (5′-HS-AAA AAA AAA AAA TAT TGA TAA GGA T-FITC-3′) were resuspended in a solution of 0.1 M dithiothreitol in 0.17 M phosphate buffer (PB) at pH 8 in order to deprotect the terminal thiol. After 1 h in the reducing environment, the oligonucleotides were desalted over a NAP-5 column (GE Healthcare). Freshly deprotected oligonucleotides (4 nmol) in Nanopure water (250 μL) were added to 1 mL of gold colloid in a glass EPA vial. The solution was shaken at 120 rpm for 16−20 h prior to salt stabilization. The oligo-AuNP solution was buffered to a pH of 7.2 with a final concentration of 10 mM PB and 0.01% SDS. The mixture was then allowed to equilibrate for 30 min before bringing the NaCl concentration to 1.0 M over an 8 h period in a stepwise manner. The solutions were sonicated to keep the particles dispersed during the salting procedure. Following salting, the particles were shaken at 120 rpm for an additional 16−20 h to yield fully functionalized oligo-AuNPs. To verify that the oligo-AuNPs were fully functionalized, we measured the loadings[10] on particles stabilized at 0.1, 0.2, 0.3, 0.4, 0.5, 0.6, 0.7, 0.8, 0.9, 1.0, 1.5, and 2.0 M NaCl. Indeed, above 0.9 M NaCl, there is no significant increase in oligonucleotide loading (Figure 1). Finally, to remove all unbound oligonucleotides from the oligo-AuNPs, the conjugates were washed by sequential centrifugation, supernatant removal, and resuspension (0.01% SDS in water). This procedure was repeated four times. Additionally, planar thin film gold surfaces[30] were functionalized with oligonucleotides in a manner almost identical to that used for the AuNPs by immersing them in a 1 mL solution of water with 4 nmol of oligonucleotide. The substrates were salted in the same manner as the particles and cleaned by successive dipping into 50 mL of 0.01% SDS in water.

Oligonucleotide Functionalized Gold Nanorod Preparation. Lyophilized oligonucleotides were resuspended in a solution 0.1 M dithiothreitol in 0.17 M PB at pH 8 in order to reduce the terminal thiols of the modified ssDNA. After 1 h in the reducing environment, the oligonucleotides were desalted over a NAP-5 column (GE Healthcare). Approximately 2 ODs (~6 nmol) of purified oligonucleotides were combined with the rod solution (~10 fM). After 30 min, the solution was buffered to 0.01% SDS, 10 mM PB, and 1.0 M NaCl over 3 h. The final solution was shaken for 48 h at 1000 rpm, at 23 °C on a thermomixer (Eppendorf, Inc.) prior to use.

Measuring Oligonucleotide Loading on Gold Nanoparticles. Freshly cleaned oligo-AuNPs were resuspended in a solution of 10 mM PB, 0.01% SDS, and 0.3 M NaCl, and 100 μL of each sample was placed in a 96-well fluorescence compatible microtiter plate. The extinction of each sample was measured on a Thermo UV−vis plate spectrophotometer at 530 nm. To determine the concentration of each AuNP sample, an extinction coefficient at 530 nm was determined for each particle size (10 nm [1.06×10^8], 15 nm [4.30×10^8], 20 nm [8.60×10^8], 30 nm [3.01×10^9], 40 nm [6.69×10^9], 50 nm [1.34×10^{10}], 60 nm [2.32×10^{10}], 80 nm [5.47×10^{10}], 100 nm [1.08×10^{11}], 150 nm [3.54×10^{11}], and 200 nm [8.60×10^{11}]). This was done by measuring the absorbance at 530 nm of a 100 μL sample of unfunctionalized gold nanoparticles on the same UV−vis plate reader and relating it to known particle concentrations. Additionally, known concentrations of fluorophore-labeled DNA (100 μL) were placed in the microtiter plate, and 100 μL of 1.0 M DTT in water was added to each well of the microtiter plate. After liberation of the thiolated oligonucleotides from the surface of the AuNPs (overnight), the total fluorescence of each well was measured on a fluorescence plate reader (FluorDia T70, Otsuka Electronics) and converted to a concentration by comparison to a standard curve. By measuring the concentration of oligonucleotides and AuNPs in each sample (five times), an average number of oligonucleotides per particle was calculated (Table 1). The loading of oligonucleotides on gold nanoparticles was also determined in the same manner as that used for the gold nanorods (see below) to ensure that the error introduced by the measurement techniques was minimized.

Measuring Oligonucleotide Loading on Gold Nanorods. A sample of oligo-functionalized nanorods was prepared as described above. An aliquot of these rods was then washed three times in 0.01% SDS, resuspended in 35 μL of 0.1 M aqueous solution of KCN, and allowed to react for 1 h in order to completely dissolve the gold rod. The resulting sample was analyzed by inductively coupled plasma mass spectrometry (ICP-MS) to determine the amount of gold. Rod concentration was determined by calculating the average number of gold atoms per nanorod (*d* = 35 nm, *l* = 475 nm, 2.43×10^7 atoms) and dividing the total amount of gold present in the dissolved sample by the number of gold atoms per nanorod. The number of oligonucleotides from this aliquot was quantified using the Oligreen assay (Invitrogen, Inc.) in a manner similar to that described above for the AuNPs. By coupling the rod concentration obtained from ICP-MS with results from the Oligreen assay, the average number of ssDNA oligonucleotides on a single nanorod could be determined (3300 ± 110 strands per rod).

Statistical Analysis. The loading of oligonucleotides on all nanoparticle sizes was conducted five times independently. Each independent trial was done by dividing the sample into three aliquots which were measured successively to limit instrumental and operator error, which averaged 7% over all of trials. The mean of the three aliquot values per trial was used to calculate the run to run mean and the standard deviations, which are shown in Table 1. From there, a percentage standard error was calculated for each particle size and was carried through the other analyses. It should be noted that the exact particle sizes as determined by the manufacturer are 9.2 ± 10% (10 nm), 14.8 ± 10% (15 nm), 19.5 ± 8% (20 nm), 29.5 ± 8% (30 nm), 39.5 ± 8% (40 nm), 48.9 ± 8% (50 nm), 61.8 ± 10% (60 nm), 78.9 ± 8% (80 nm), 101.6 ± 8% (100 nm), 152.6 ± 8% (150 nm), and 203.2 ± 8% (200 nm). It should be noted that these values were used to calculate the average surface coverage of oligonucleotides, deflection angles, and footprint values in Table 1.

Acknowledgment. The authors thank Andrew Senesi for providing the gold substrates, and Robert Macfarlane for assistance with the DLS. C.A.M. acknowledges the NU-NSEC (sponsored by the NSF) and NCI-CCNE for support of the work. He is also grateful for a NIH Director's Pioneer Award. H.D.H. acknowledges the U.S. Department of Homeland Security (DHS) for a Graduate Fellowship under the DHS Scholarship and Fellowship Program. J.E.M. acknowledges a Northwestern University Presidential Fellowship for support.

REFERENCES AND NOTES

1. Alivisatos, P. The Use of Nanocrystals in Biological Detection. *Nat. Biotechnol.* **2004**, *22*, 47–52.
2. Daniel, M. C.; Astruc, D. Gold Nanoparticles: Assembly, Supramolecular Chemistry, Quantum-Size-Related Properties, and Applications toward Biology, Catalysis, and Nanotechnology. *Chem. Rev.* **2004**, *104*, 293–346.
3. Niemeyer, C. M. Nanoparticles, Proteins, and Nucleic Acids: Biotechnology Meets Materials Science. *Angew. Chem., Int. Ed.* **2001**, *40*, 4128–4158.
4. Rosi, N. L.; Mirkin, C. A. Nanostructures in Biodiagnostics. *Chem. Rev.* **2005**, *105*, 1547–1562.
5. Chang, M. M. C.; Cuda, G.; Bunimovich, Y. L.; Gaspari, M.; Heath, J. R.; Hill, H. D.; Mirkin, C. A.; Nijdam, A. J.; Terracciano, R.; Thundat, T.; *et al.* Nanotechnologies for Biomolecular Detection and Medical Diagnostics. *Curr. Opin. Chem. Biol.* **2006**, *10*, 11–19.
6. Taton, T. A.; Mirkin, C. A.; Letsinger, R. L. Scanometric DNA Array Detection with Nanoparticle Probes. *Science* **2000**, *289*, 1757–1760.
7. Rosi, N. L.; Giljohann, D. A.; Thaxton, C. S.; Lytton-Jean, A. K. R.; Han, M. S.; Mirkin, C. A. Oligonucleotide-Modified Gold Nanoparticles for Intracellular Gene Regulation. *Science* **2006**, 1027–1030.

8. Giljohann, D. A.; Seferos, D. S.; Patel, P. C.; Millstone, J. E.; Rosi, N. L.; Mirkin, C. A. Oligonucleotide Loading Determines Cellular Uptake of DNA-Modified Gold Nanoparticles. *Nano. Lett.* **2007**, *7*, 3818–3821.
9. Lytton-Jean, A. K. R.; Mirkin, C. A. A. Thermodynamic Investigation into the Binding Properties of DNA Functionalized Gold Nanoparticle Probes and Molecular Fluorophore Probes. *J. Am. Chem. Soc.* **2005**, *127*, 12754–12755.
10. Hurst, S. J.; Lytton-Jean, A. K. R.; Mirkin, C. A. Maximizing DNA Loading on a Range of Gold Nanoparticle Sizes. *Anal. Chem.* **2006**, *78*, 8313–8318.
11. Luedtke, W. D.; Landman, U. Structure, Dynamics, and Thermodynamics of Passivated Gold Nanocrystallites and Their Assemblies. *J. Phys. Chem.* **1996**, *100*, 13323–13329.
12. Luedtke, W. D.; Landman, U. Structure and Thermodynamics of Self-Assembled Monolayers on Gold Nanocrystallites. *J. Phys. Chem. B* **1998**, *102*, 6566–6572.
13. Bloomfield, V. A. C., D. M.; Tinoco, J. I. *Nucleic Acids: Structures, Properties, and Functions*; University Science Books: Sausalito, CA, 2000.
14. Smith, S. B.; Cui, Y.; Bustamante, C. Overstretching B-DNA: The Elastic Response of Individual Double-Stranded and Single-Stranded DNA Molecules. *Science* **1996**, *271*, 795–799.
15. Banholzer, M. J.; Li, S.; Ketter, J. B.; Rozkiewicz, D. I.; Schatz, G. C.; Mirkin, C. A. Electrochemical Approach to and the Physical Consequences of Preparing Nanostructures from Gold Nanorods with Smooth Ends. *J. Phys. Chem. C* **2008**, *112*, 15729–15734.
16. Lee, J.-S.; Seferos, D. S.; Giljohann, D. A.; Mirkin, C. A. Thermodynamically Controlled Separation of Polyvalent 2-nm Gold Nanoparticle-Oligonucleotide Conjugates. *J. Am. Chem. Soc.* **2008**, *130*, 5430–5431.
17. Bao, Y. P.; Huber, M.; Wei, T. F.; Marla, S. S.; Storhoff, J. J.; Muller, U. R. SNP Identification in Unamplified Human Genomic DNA with Gold Nanoparticle Probes. *Nucleic Acids Res.* **2005**, *33*, e15.
18. Dillenback, L. M.; Goodrich, G. P.; Keating, C. D. Temperature-Programmed Assembly of DNA:Au Nanoparticle Bioconjugates. *Nano. Lett.* **2006**, *6*, 16–23.
19. Elghanian, R.; Storhoff, J. J.; Mucic, R. C.; Letsinger, R. L.; Mirkin, C. A. Selective Colorimetric Detection of Polynucleotides Based on the Distance-Dependent Optical Properties of Gold Nanoparticles. *Science* **1997**, *277*, 1078–1081.
20. Huang, C. C.; Huang, Y. F.; Cao, Z. H.; Tan, W. H.; Chang, H. T. Aptamer-Modified Gold Nanoparticles for Colorimetric Determination of Platelet-Derived Growth Factors and Their Receptors. *Anal. Chem.* **2005**, *77*, 5735–5741.
21. Witten, K. G.; Bretschneider, J. C.; Eckert, T.; Richtering, W.; Simon, U. Assembly of DNA-Functionalized Gold Nanoparticles Studied by UV/Vis-Spectroscopy and Dynamic Light Scattering. *Phys. Chem. Chem. Phys.* **2008**, *10*, 1870–1875.
22. Kim, A. J.; Biancaniello, P. L.; Crocker, J. C. Engineering DNA-Mediated Colloidal Crystallization. *Langmuir* **2006**, *22*, 1991–2001.
23. Liu, J. W.; Lu, Y. A Colorimetric Lead Biosensor Using DNAzyme-Directed Assembly of Gold Nanoparticles. *J. Am. Chem. Soc.* **2003**, *125*, 6642–6643.
24. Nykypanchuk, D.; Maye, M. M.; van der Lelie, D.; Gang, O. DNA-Guided Crystallization of Colloidal Nanoparticles. *Nature* **2008**, *451*, 549–552.
25. Park, S. Y.; Lytton-Jean, A. K. R.; Lee, B.; Weigand, S.; Schatz, G. C.; Mirkin, C. A. DNA-Programmable Nanoparticle Crystallization. *Nature* **2008**, *451*, 553–556.
26. Sam, M.; Boon, E. M.; Barton, J. K.; Hill, M. G.; Spain, E. M. Morphology of 15-mer Duplexes Tethered to Au(111) Probed Using Scanning Probe Microscopy. *Langmuir* **2001**, *17*, 5727–5730.
27. Beaucage, S. L.; Caruthers, M. H. Deoxynucleoside Phosphoramidites-A New Class of Key Intermediates for Deoxypolynucleotide Synthesis. *Tetrahedron Lett.* **1981**, *22*, 1859–1862.
28. Martin, C. R. Nanomaterials: A Membrane-Based Synthetic Approach. *Science* **1994**, *266*, 1961–1966.
29. Routkevitch, D.; Bigioni, T.; Moskovits, M.; Xu, J. M. Electrochemical Fabrication of CdS Nanowire Arrays in Porous Anodic Aluminum Oxide Templates. *J. Phys. Chem.* **1996**, *100*, 14037–14047.
30. Love, J. C.; Estroff, L. A.; Kriebel, J. K.; Nuzzo, R. G.; Whitesides, G. M. Self-Assembled Monolayers of Thiolates on Metals as a Form of Nanotechnology. *Chem. Rev.* **2005**, *105*, 1103–1169.